# NATIONAL ADVISORY COMMITTEE FOR AERONAUTICS

TECHNICAL NOTE 2691

THEORETICAL AND EXPERIMENTAL ANALYSIS OF ONE-DIMENSIONAL COMPRESSIBLE FLOW IN A

ROTATING RADIAL-INLET

IMPELLER CHANNEL

By Seymour Lieblein

Lewis Flight Propulsion Laboratory Cleveland, Ohio

PROPERTY FAIRCHILD

NACA

Washington

April 1952

#### NATIONAL ADVISORY COMMITTEE FOR AERONAUTICS

#### TECHNICAL NOTE 2691

THEORETICAL AND EXPERIMENTAL ANALYSIS OF ONE-DIMENSIONAL COMPRESSIBLE

FLOW IN A ROTATING RADIAL-INLET IMPELLER CHANNEL

By Seymour Lieblein

#### SUMMARY

An analysis of the one-dimensional compressible flow in a rotating radial-plane impeller channel was conducted in order to provide an insight into the characteristics of the passage mean flow under the influence of centrifugal forces and losses. From a theoretical investigation of the flow in an illustrative impeller channel with convergent-divergent area variation, the behavior of the flow along the channel was found to be generally similar in trend to the flow in a stationary convergent-divergent nozzle. The critical (sonic) section of the rotating channel occurred upstream of the geometric throat. The effect of the losses on the flow was similar to the effect of a reduction of the flow area.

A further one-dimensional analysis was conducted of the flow in an experimental radial-inlet impeller containing static-pressure taps along the stationary front shroud. The behavior of the mean flow along the impeller passage was generally similar to that of the flow along a rotating radial channel in which the effective flow area in the inlet region varied with the operating point. At negative angles of attack, sonic velocity was attained in the inlet region of the impeller where a throat had formed because of the separation of the flow. Calculated maximum weight flows based on conditions at the critical radius compared favorably with experimental maximum weight flows over the wheel-speed range of the impeller. Impeller-inlet losses were found to be large at the higher weight flows.

#### INTRODUCTION

In an attempt to understand the fundamental-flow behavior of centrifugal compressors, several theoretical and experimental investigations of the flow within centrifugal-impeller passages have recently been conducted (references 1 to 6). Considerable attention has been given to the two-dimensional impeller types with radial inlet and discharge, in particular. These studies have included experimental measurements of over-all performance and passage flow (references 3 to 5) and theoretical calculations of passage and blade-surface flow distributions (references 1, 2, and 6).

One of the characteristics of these impeller analyses is the assumption that the flow proceeds without loss and completely fills the geometric area of the passage at all times. Experimental results have indicated, however, that, particularly in the inlet regions of impellers, friction and mixing losses and boundary-layer separation exert significant effects on the behavior of the channel flow.

As a preliminary approach to the incorporation of such "real-flow" effects in an impeller analysis, the usefulness of one-dimensional considerations in studying the actual passage mean flow of impeller channels was investigated at NACA Lewis laboratory. A one-dimensional analysis is helpful for evaluating the various types of losses, for locating regions of large loss, and as an initial basis for the introduction of friction and loss terms in theoretical developments. For methods of analysis such as in references 4 and 6, the use of more realistic passage mean flows could result in more accurate determinations of velocity distributions along blade surfaces.

An academic analysis of the ideal flow in a rotating radial-plane channel whose area variation was selected to represent the effective flow area existing in experimental impellers is presented in the first part of this report. Based on an illustrative impeller channel, the effects of centrifugal force and losses on the general one-dimensional flow variation and on such factors as location of the critical section, maximum mass flow, and shock formation are investigated.

In the second part of this report, the one-dimensional analysis is applied in conjunction with impeller front-shroud static-pressure measurements to an investigation of the flow in the passages of a radial-inlet impeller whose over-all performance was reported in reference 5. The general variations of the flow are discussed, and calculation of the effective flow area in the impeller-inlet region is made. The choking of the impeller flow and variations of impeller losses are analyzed.

#### SYMBOLS

The following symbols are used herein:

- A area
- a velocity of sound
- c<sub>p</sub> specific heat at constant pressure
- E energy number  $\left(E^2 = -\frac{VdV}{\frac{dp}{\rho}}\right)$

- F energy loss or work done in overcoming losses
- g acceleration due to gravity
- J mechanical equivalent of heat
- K constant
- M flow Mach number
- Mt impeller-tip Mach number (tip speed/a<sub>0</sub>)
- n polytropic exponent
- P absolute total pressure
- p static pressure
- Q heat energy added
- R gas constant
- r impeller radius
- T absolute total temperature
- t static temperature
- V relative velocity
- W mass flow
- w weight flow
- a angle of attack
- γ ratio of specific heats
- 8 ratio of inlet total pressure to standard sea-level pressure
- η<sub>ad</sub> adiabatic efficiency
- θ ratio of inlet total temperature to standard sea-level temperature
- ρ mass density
- ₩ flow function

w angular velocity

Subscripts:

l impeller inlet

c critical (sonic) condition

m maximum

o inlet total (stagnation) conditions

T impeller tip

t throat

The prime refers to irreversible (loss) conditions.

#### THEORETICAL ANALYSIS

# Basic Equations

In a one-dimensional theory of the steady flow of a perfect gas in a channel, the state of the fluid is considered to be sufficiently defined by average values of its components such that each flow variable is a function of a single parameter or coordinate of position. The conventional variables - pressure p, temperature t, density  $\rho$ , and relative velocity V - as functions of a single space parameter in steady flow are connected by four relations derived in reference 7, which when altered to include the effect of the centrifugal force field of a rotating passage are given by:

Conservation of energy

$$VdV + c_p J dt - dQ - d\left(\frac{\omega^2 \mathbf{r}^2}{2}\right) = 0$$
 (1)

Conservation of mass

$$d(\rho VA) = 0 \tag{2}$$

Equation of motion

$$\frac{\mathrm{dp}}{\rho} + V \, \mathrm{d}V + \mathrm{d}F - \mathrm{d}\left(\frac{\omega^2 \mathbf{r}^2}{2}\right) = 0 \tag{3}$$

Equation of state

$$d(p/\rho Rt) = 0 (4)$$

The variations of pressure, relative velocity, and relative Mach number along the radius of a channel are then obtained from equations (1) to (4) (appendix A) as the logarithmic differential equations

$$\frac{\mathrm{d}p}{p} = \frac{\gamma}{1-M^2} \left( \frac{1}{a^2} \left\{ \mathrm{d} \left( \frac{\omega^2 \mathbf{r}^2}{2} \right) - \left[ (\gamma - 1) M^2 + 1 \right] \mathrm{d}\mathbf{F} - (\gamma - 1) M^2 \mathrm{d}\mathbf{Q} \right\} + M^2 \frac{\mathrm{d}\mathbf{A}}{\mathbf{A}} \right)$$
(5)
$$\frac{\mathrm{d}V}{V} = -\frac{1}{1-M^2} \left\{ \frac{1}{a^2} \left[ \mathrm{d} \left( \frac{\omega^2 \mathbf{r}^2}{2} \right) - \gamma \mathrm{d}\mathbf{F} - (\gamma - 1) \mathrm{d}\mathbf{Q} \right] + \frac{\mathrm{d}\mathbf{A}}{\mathbf{A}} \right\}$$
(6)
$$\frac{\mathrm{d}M}{M} = -\frac{1}{2(1-M^2)} \left( \frac{1}{a^2} \left\{ (1+\gamma) \mathrm{d} \left( \frac{\omega^2 \mathbf{r}^2}{2} \right) - \gamma \right\} \right)$$
(7)
$$\gamma \left[ 2 + (\gamma - 1) M^2 \right] \mathrm{d}\mathbf{F} - (\gamma - 1) (1 + \gamma M^2) \mathrm{d}\mathbf{Q} \right\} + \left[ 2 + (\gamma - 1) M^2 \right] \frac{\mathrm{d}\mathbf{A}}{\mathbf{A}}$$
(7)

The variations of velocity, pressure, and Mach number are thus seen to be functions of the individual contributions of the gradients of wheel potential energy, friction loss, heat transfer, and flow area with the square of the Mach number as the principal parameter.

For isentropic flow along a rotating impeller channel (dF = 0, dQ = 0), the equations of motion and energy become identical. The ideal state of flow at any radius is then obtained by integrating equation (3) isentropically between the inlet of the channel and a point in the channel to yield

$$\frac{\mathbf{v}^{2}}{2} + \frac{\gamma}{\gamma - 1} \frac{\mathbf{p}}{\rho} - \frac{\omega^{2} \mathbf{r}^{2}}{2} = \frac{\mathbf{v}_{1}}{2} + \frac{\gamma}{\gamma - 1} \frac{\mathbf{p}_{1}}{\rho_{1}} - \frac{\omega^{2} \mathbf{r}_{1}^{2}}{2}$$
(8)

If there is no prerotation at the inlet to the rotating passage, the velocity terms on the right side of the equation are equal to the kinetic energy of the absolute velocity immediately before the entrance to the rotating channel, so that

$$\frac{\mathbf{v}^2}{2} + \frac{\mathbf{r}}{\mathbf{r} - \mathbf{l}} \frac{\mathbf{p}}{\rho} - \frac{\omega^2 \mathbf{r}^2}{2} = c_p J \mathbf{T}_1 \tag{9}$$

Making use of equation (4) and the isentropic relations,

$$T_1 = T_0$$

$$\frac{P}{\rho^{\gamma}} = \frac{P}{\rho_0^{\gamma}}$$

$$a_0^2 = \gamma \frac{P}{\rho_0}$$

Equation (9) can be written in terms of stagnation conditions upstream of the channel inlet as

$$\frac{\Upsilon^{-1}}{2} \frac{V^{2}}{a_{O}^{2}} + \left(\frac{P}{P_{O}}\right)^{\Upsilon} = 1 + \frac{\Upsilon^{-1}}{2} \left(\frac{r}{r_{T}}\right)^{2} M_{T}^{2}$$
 (10)

where  $M_T$  is defined as impeller-tip Mach number and is equal to  $\omega r_T/a_0$ . The ideal state of flow can then be calculated at any point along the channel over a range of rotational speeds and weight flows by the use of equation (10) in conjunction with the continuity condition.

The applicability of the general validity of the one-dimensional approximation (equations (5) to (7), or (10)) depends on the degree of variation of flow conditions across a plane normal to the direction of flow. The velocity variations in impeller channels (because of blade loading, secondary flows, and boundary layers) are recognized as being greater than those normally encountered in tubes and nozzles for which the one-dimensional assumption has been found adequate. Calculations of energy and efficiency based on full channel area and average velocity would therefore contain inherent inaccuracy. However, if the number of blades is large and if corrections for effective flow area are made, the one-dimensional approximation might yield reliable information concerning the variation of the average flow along the radius of a rotating channel.

# Flow in Illustrative Impeller Channel

The principal effects of energy transfer and area variation on the basic behavior and restriction of the flow in rotating channels can best be demonstrated by first investigating the flow of an ideal isentropic fluid and illustrating the analysis for a representative channel. The effects of losses and friction can then be examined as causing departures from the ideal configurations.

Geometry of channel. - The radial variation of geometric area normal to the relative flow path for the illustrative impeller channel was selected to represent the effective flow-area variations existing in the channels of the radial impellers used in references 3 and 5. The geometric area of these impellers was designed to increase along the flow path from inlet to outlet. In the inlet region of the impeller, the true flow area is not clearly defined because of the variation of the magnitude of the relative area of the approaching air as the impeller weight flow is varied. As shown in figure 1, at low weight flows, the relative approach area is less and at high weight flow, the relative approach area is greater than the blade-inlet area. A continuous variation of area must occur across the inlet, however, as the flow adjusts to the channel shape. At the high weight flows, for example, the adjustment involves a separation of flow from the driving surface, the formation of a throat, and then mixing and reattachment of the flow. Evidence of inlet-area reduction in experimental radial impellers at high weight flow is found in references 3 to 5. In order, therefore, to employ a fixed-area variation representative of the effective flow area of experimental impeller channels, a convergent-divergent configuration was chosen for the illustrative channel. For convenience, a parabolic variation of area was prescribed. The area variation, equivalent circular nozzle and general configuration of the fictitious impeller corresponding to this area variation with negligible axial curvature, is shown in figure 2. Although the effective throat in the experimental impeller does not occur as far downstream as indicated in figure 2, the exaggerated theoretical location was chosen to accent the effects of the throat formation. Blade thickness in figure 2(c) represents both actual blade and separated areas. The fluid is assumed to follow the mean flow path between blades (direction for infinite number of blades) and to completely fill the passage at all times. Inlet, throat, and discharge sections of the channel are shown by stations 1, t, and T, respectively. Stagnation conditions are assumed at station o.

Description of flow. - The state of flow along the channel of the illustrative impeller (fig. 2) was calculated over a range of rotational speeds and mass flows by means of equation (10) and the continuity condition. The variations with radius ratio of pressure ratio, velocity, and Mach number for increasing rates of flow from zero to maximum are shown in figure 3 for an impeller-tip Mach number of 1.0. The trends of variation of pressure, velocity, and Mach number are thus seen in general to be similar to those of a stationary convergent-divergent nozzle. The instantaneous rise in pressure at the blade inlet is due to the fact that the angle of the arbitrarily defined blade shape at the inlet does not correspond to the angles of the entering air at the rotational speed chosen. When the flow is assumed to follow the mean blade angle, an instantaneous change in flow angle and velocity occurs which results in an instantaneous rise in the absolute tangential velocity.

Unlike the flow in a stationary nozzle, the location of the points of minimum pressure, maximum velocity, and maximum Mach number in a rotating channel are not coincident and occur upstream of the geometric throat. The dashed lines in figure 3 connects the points of minimum and maximum values.

The variation of the locations of the flow minimums and maximums is apparent from an inspection of the basic differential equations (5) to (7) from which the following equations are obtained for zero slopes of p, V, and M in isentropic flow:

Minimum pressure

$$\left(\frac{\mathbf{r}}{\mathbf{A}}\frac{\mathrm{dA}}{\mathrm{d}\mathbf{r}}\right)_{\mathrm{p}} = -\frac{\left(\frac{\mathbf{r}}{\mathbf{r}_{\mathrm{T}}}\right)^{2} M_{\mathrm{T}}^{2} \left(1 + \frac{\Upsilon - 1}{2} M^{2}\right)}{M^{2} \left[1 + \frac{\Upsilon - 1}{2} \left(\frac{\mathbf{r}}{\mathbf{r}_{\mathrm{T}}}\right)^{2} M_{\mathrm{T}}^{2}\right]} \tag{11a}$$

Maximum velocity

$$\left(\frac{\mathbf{r}}{\mathbf{A}}\frac{\mathrm{dA}}{\mathrm{dr}}\right)_{\mathbf{V}} = -\frac{\left(\frac{\mathbf{r}}{\mathbf{r}_{\mathbf{T}}}\right)^{2} \mathbf{M}_{\mathbf{T}}^{2} \left(1 + \frac{\mathbf{\gamma} - 1}{2} \mathbf{M}^{2}\right)}{\left[1 + \frac{\mathbf{\gamma} - 1}{2} \left(\frac{\mathbf{r}}{\mathbf{r}_{\mathbf{T}}}\right)^{2} \mathbf{M}_{\mathbf{T}}^{2}\right]}$$
(11b)

Maximum Mach number

$$\left(\frac{\mathbf{r}}{\mathbf{A}}\frac{\mathrm{dA}}{\mathrm{dr}}\right)_{\mathrm{M}} = -\frac{\frac{\Upsilon+1}{2}\left(\frac{\mathbf{r}}{\mathbf{r}_{\mathrm{T}}}\right)^{2} M_{\mathrm{T}}^{2}}{\left[1 + \frac{\Upsilon-1}{2}\left(\frac{\mathbf{r}}{\mathbf{r}_{\mathrm{T}}}\right)^{2} M_{\mathrm{T}}^{2}\right]} \tag{11c}$$

In the development of equations (11), use was made of the equation

$$a^{2} = a_{0}^{2} \left[ \frac{1 + \frac{\Upsilon - 1}{2} \left( \frac{r}{r_{T}} \right)^{2} M_{T}^{2}}{1 + \frac{\Upsilon - 1}{2} M^{2}} \right]$$

which was derived from the general energy equation with the ratio of temperatures related to the ratio of the velocities of sound.

The locations of minimum pressure and maximum velocity therefore apparently vary with the local flow Mach number as well as the channel geometry and rotor Mach number, but the maximum local Mach number location is independent of flow. At the critical value of flow Mach number (M = 1), the locations of the pressure and velocity become coincident at the critical section.

The location of the critical radius (M = 1) varies with both the rotor Mach number and the rate of convergence of the channel. With the use of a parabolic variation of area, several rates of convergence between the inlet and throat sections of the illustrative channel were obtained as the ratio of throat area to inlet area at constant throat area was varied. The effect of the rate of convergence and rotor Mach number on the location of the critical radius ratio is shown in figure 4. The curves illustrate the general consideration that because the contraction and energy effects are in opposition, the largest displacements are to be expected for low rates of convergence and for high values of rotor Mach number.

Maximum mass flow. - The maximum mass flow that a cross section of the channel is capable of passing under isentropic conditions is found by differentiating the expression for mass flow with respect to pressure ratio at the section and setting the derivative equal to zero. From this development (appendix B) it is found that the maximum mass flow occurs at the critical condition where the flow Mach number is l and the pressure ratio is given by

$$\left(\frac{p}{P_{O}}\right)_{c} = \left[\frac{2}{\gamma+1} + \frac{\gamma-1}{\gamma+1} \left(\frac{r}{r_{T}}\right)_{c}^{2} M_{T}^{2}\right]^{\frac{\gamma}{\gamma-1}}$$
(12)

For radial flow with rotation, the critical pressure ratio increased with increasing impeller-tip Mach number. With no rotation, equation (12) reduces to the well-known value for critical pressure ratio of 0.528 for energy-conservative systems ( $\gamma = 1.40$ ). The variation of critical pressure ratio with impeller-tip Mach number is shown in figure 5 for the illustrative channel.

The increase in critical density corresponding to the increase in critical pressure (fig. 5) indicates that the channel is capable of passing a greater mass of fluid as the rotor Mach number is increased. The variation of maximum mass flow as described by the flow function \( \psi is given by (appendix B)

$$\psi_{\rm m} = \frac{W_{\rm m}}{\rho_{\rm o} a_{\rm o} A_{\rm c}} = \left\{ \frac{2}{\gamma + 1} \left[ 1 + \frac{\gamma - 1}{2} \left( \frac{r}{r_{\rm T}} \right)_{\rm c}^2 M_{\rm T}^2 \right] \right\} \frac{\frac{\gamma + 1}{2(\gamma - 1)}}{(13)}$$

The relation for the illustrative channel is shown in figure 6. The increase in maximum mass flow results not only from the increase in density but also from the increase in critical area as the critical section moves upstream from the throat. The curve of the maximum mass-flow function (fig. 6) is actually the locus of the maximum points of the curves of variation of flow function with pressure ratio at various rotor Mach numbers. The general value of  $\psi$  as obtained from equation (B7) of appendix B is

$$\psi = \sqrt{\frac{2}{\Upsilon^{-1}} \left\{ \left[ 1 + \frac{\Upsilon^{-1}}{2} \left( \frac{\mathbf{r}}{\mathbf{r}_{\mathrm{T}}} \right)^{2} M_{\mathrm{T}}^{2} \right] \left( \frac{\mathbf{p}}{\mathbf{P}_{\mathrm{O}}} \right)^{\Upsilon} - \left( \frac{\mathbf{p}}{\mathbf{P}_{\mathrm{O}}} \right)^{\Upsilon} \right\}}$$
(14)

The complete mass-flow spectrum for the illustrative channel up to an impeller tip Mach number of 1.8 is plotted in figure 7.

Supersonic flow. - For values of outlet static pressure lower than that required for continuous isentropic compression at the critical mass flow, supersonic velocities are obtained in the passage downstream of the critical section. As in the flow through stationary nozzles, the fluid expands isentropically to some point downstream of the critical section, passes through a normal compression shock, and is then further compressed isentropically to the prevailing outlet pressure. The location and strength of the shock are determined by the magnitude of the outlet pressure. The variation of static-pressure ratio and shock location in the supersonic-flow region of the illustrative channel is shown in figure 8 for several supercritical outlet pressures. The dashed lines are curves of constant entropy corresponding to the various outlet pressures. The shock location for a given supercritical outlet pressure was determined by comparing the static-pressure ratio from the constant-entropy curve for that supercritical pressure to the isentropic expansion curve with the static-pressure ratio that would occur across a normal shock located at the particular radial position.

An examination of the equations of motion and the entropy relation (as was done in reference 8) for flow with energy transfer due to radius change revealed that shocks are both mechanically and thermodynamically possible in the region between the critical section and the throat. Aside from the difference in location between the geometric and aerodynamic throats, all conventional theoretical supersonic flow and normal shock relations are valid for one-dimensional radial impeller flow. In the real impeller flow with finite shock thickness, the energy transfer may have some effect on shock stability, boundary-layer interaction, and flow separation.

Losses. - In the actual flow in channels of radial impellers, the existence of internal losses arising from friction, turbulence, and

NACA TN 2691

mixing will modify to some extent the general picture of the flow behavior obtained in the previous sections. From equations (5) to (7), for adiabatic flow the effect of losses (by means of entropy and static-temperature increases) accelerated the flow along the channel, or in other words, losses can generally be considered to have the effect of a reduction in the flow area. As such, the critical radius, as well as the locations of minimum pressure and maximum velocity, will be displaced downstream nearer the geometric throat.

The critical condition in the presence of losses continues to be characterized by the attainment of a relative Mach number of 1 as indicated by the singularity in equations (5) to (7) at M = 1. In the presence of losses, the pressure ratio at which sonic velocity occurs will be reduced and a corresponding reduction in maximum mass flow will occur. The variation of maximum mass flow with critical pressure ratio (known as the choking line) for radial impeller flow expressed as the ratio of the mass-flow function at any irreversible condition to the ideal isentropic mass-flow function was found (appendix C) to be

$$\frac{\psi_{c}^{'}}{\psi_{c}} = \frac{\left(\frac{\underline{p}'}{P_{o}}\right)_{c}}{\left(\frac{\underline{p}}{P_{o}}\right)_{c}} \frac{\sqrt{1 + \frac{\Upsilon - 1}{2} \left(\frac{\underline{r}'}{r_{T}}\right)_{c}^{2} M_{T}^{2}}}{\sqrt{1 + \frac{\Upsilon - 1}{2} \left(\frac{\underline{r}}{r_{T}}\right)_{c}^{2} M_{T}^{2}}}$$
(15)

The maximum mass flow is, therefore, a function also of the location of the critical section and its variation with the losses.

A relatively large effect of losses on the general flow behavior occurs when the channel flow involves a breakaway of the boundary layer or the formation of eddy regions. In such cases, the geometric-area variation of the channel can no longer be considered as the actual area governing the flow. For a given impeller channel, the variation of the actual flow area can be related to the principal flow variables from combination of the equation of continuity (equation (2)) and

$$a^2 = \frac{\gamma p}{\rho} = \frac{\gamma}{n} \frac{dp}{d\rho}$$

where n is the polytropic exponent, as

$$\frac{dA}{A} = -\frac{dp}{a^{2}\rho} \left( \frac{1}{M^{2}} \frac{V \, dV}{\frac{dp}{Q}} + \frac{\gamma}{n} \right) \tag{16}$$

At this point, the concept of an energy number is introduced. The energy number is defined so that its square is equal to minus the ratio of the rate of change along the flow path of kinetic energy to the rate of change of static enthalpy, or

$$E^2 = -\frac{V \, dV}{\frac{dp}{\rho}}$$

Equation (16) can therefore be expressed as

$$\frac{dA}{A} = -\frac{dp}{\gamma p} \left( \frac{\gamma}{n} - \frac{E^2}{M^2} \right)$$

and, when the minimum or maximum of the flow area develops, the condition will be characterized by

$$M^2 = \frac{n}{\gamma} E^2 \tag{17}$$

Inasmuch as in most cases the effect on the average flow variation of the area reduction (which was due to breakaway) will be greater than the entropy increase accompanying the separation, the condition can be represented very closely by the simple relation

$$M^2 = E^2 \tag{18}$$

Thus an intersection of the curves of the squares of Mach number and energy number along the channel should reveal the presence and location of a minimum or maximum of the actual flow area.

#### EXPERIMENTAL ANALYSIS

The use of one-dimensional theory in the investigation of the mean flow in channels of centrifugal impellers is illustrated by an analysis of the flow in the radial-inlet impeller of reference 5.

# Apparatus

A photograph of the radial-inlet impeller is shown in figure 9. The direction of the flow at the entrance to and along the impeller was confined predominantly in a radial plane. The impeller contained 18 blades and had an outer diameter of 14 inches. The impeller investigation was conducted in a variable-component test setup with a 34-inch vaneless diffuser at tip speeds from 800 to 1300 feet per second. In addition to standard performance instrumentation, static-pressure taps were installed along the impeller stationary front shroud. A complete description of the impeller design and experimental setup are given in reference 5.

#### Calculations

The average state of the air at points along the channel of the impeller were calculated for the various tip speeds from the measurements of static pressure taken along the stationary-front shroud. Because of the essentially radial nature of the impeller configuration, the variation of pressure across the depth of the passage from front to rear shroud should be negligible compared with the variations along the streamline (as was indicated in reference 3 for a geometrically similar impeller). The pressure readings along the stationary-front shroud therefore closely represent the average (one-dimensional) static pressure in the channel at each radial position. Other assumptions made in the calculations were: (1) The direction of the flow followed the curvature of the blades at all points, (2) the impeller channel was flowing full at all times, and (3) the flow was isentropic. The detailed procedure involved in the calculating of the principal flow variables from the continuity condition and energy equation (similar to equation (10)) are given in reference 5.

# Analysis of Flow

General variations. - Illustrative examples of the measured variation of static pressure along the impeller radius and the calculated variations of velocity and Mach number are shown in figure 10 for four weight flows at an impeller-tip Mach number of 0.878. Although the measured static-pressure variation with radius was not precisely defined in the inlet region of the impeller because of the few tap locations used in the investigation presented in reference 5, subsequent unpublished data from the same impeller with a considerably larger number of pressure taps along the front shroud have substantiated the faired variations used for the original data.

The plots of static pressure, velocity, and flow Mach number (fig. 10) reveal a general similarity to the flow in the illustrative convergent-divergent channel in figure 3. The effect of the formation of a throat in the inlet region due to increasing relative approach area and leading edge separation at high weight flows is apparent. In the maximum flow range, the pressure drop became quite pronounced, resulting in local Mach numbers becoming and exceeding 1. After the maximum weight flow was attained, further reductions in discharge pressure increase the magnitude of the supersonic velocities and accompanying shocks and shift the shock regions further downstream from the throat. As a result of these effects, a considerable decrease in efficiency was obtained.

Effective flow area. - In a previous section a minimum or maximum of the flow area is shown to be characterized by the equality of the squares of the local Mach number M<sup>2</sup> and the energy number E<sup>2</sup>. For the geometric-area variation of the test impeller (fig. 11), if the effective channel in the impeller-inlet region is to be considered non-rigid and varying with weight flow such that a throat forms at the higher weight flows, then the qualitative radial variation of the principal flow variables over the complete weight-flow range at constant tip speed will appear as illustrated in figure 12. The corresponding qualitative variations of Mach number and energy number will be as shown in figure 13. One intersection should be anticipated in the outlet region where the maximum geometric area occurs, and in the high flow range, a second intersection should be expected in the inlet region as the throat develops.

Values of Mach number and energy number were calculated for the test impeller based on the ideal geometric area of the impeller channel and are shown in figure 14 for the test range of flow at an impellertip Mach number of 0.878. The calculated values of  $M^2$  and  $E^2$  in general follow the qualitative variations of figure 13 rather closely. The entrance-region intersection, as expected, indicates the existence of a minimum of the flow area. The downstream shift of the minimum of the flow area with an increase in flow is also apparent. Similar variations of  $E^2$  and  $M^2$  were obtained for the runs of an impeller-tip Mach number of 0.965.

Calculations of the effective flow area which was required to pass the measured maximum weight flow and to produce the measured pressureratio variation were made for the accelerating flow region at the inlet for several impeller-tip Mach numbers. The effective flow area was determined from equation (10) in which the area A was introduced by means of the continuity substitution for the relative velocity V. A polytropic efficiency of 0.95 was assumed for the pressure-density relation. The calculated flow area in the accelerating flow region at maximum weight flow at an impeller-tip Mach number of 0.878 is shown in figure 11 in comparison with the geometric area and relative approach area in order to illustrate the nature of the effective area contraction.

Maximum weight flow. - At a given tip speed, the magnitude of the maximum weight flow resulting from the attainment of the critical conditions within the impeller passage depends on the location of the critical section and efficiency of the flow. As a first approach, ideal critical conditions were assumed. The location of the critical radius was obtained for each tip-speed run by comparing the calculated ideal-critical pressure ratio as given by equation (12) with the measured static-pressure ratios (fig. 15 for impeller-tip Mach numbers of 0.878 and 1.058). The maximum corrected weight flow at each tip speed was obtained from equation (13) and the calculated effective flow area

NACA TN 2691 15

(as in fig. 11) at the critical radius. Maximum weight flow plotted against impeller-tip Mach number is shown in figure 16 in comparison with the measured values of reference 5. As expected, the calculated maximum weight flow agreed very closely with the experimental values.

Values of maximum weight flow predicted by the conventional practice of assuming the choking to occur at the impeller inlet (vane leading edge) are also shown in figure 16. The assumption of inlet choking apparently is inaccurate for predicting maximum weight flow for this type of impeller, and an improved method based on choking at the effective throat within the passage is desirable.

In plotting the calculated effective flow area, the effective flow area at the critical radius was observed to be very nearly equal to the geometric area at all tip speeds (for example fig. 11). This was believed to be due to the consideration that, as the flow area varied from the relative approach area upstream of the inlet (greater than the geometric area) to the throat area in the separated region downstream of the inlet (smaller than the geometric area), there is some point upstream of the throat where the effective flow area is equal to the geometric area. With the critical section occurring upstream of the throat, the displacement from the throat was of sufficient magnitude to result in the near equality of the areas. Thus, for a given impeller, if the location of the critical radius can be approximated (from an inspection of the geometric-area variation and the relative approach areas), the ideal weight flow based on geometric area at the critical section may provide a method of predicting maximum weight flow that is more accurate than the inlet-choking estimate. For the radial-inlet impeller of reference 5, ideal maximum weight flow based on geometric area at the critical section is shown by the dashed line in figure 16.

Losses and efficiency. - The measured variation of over-all efficiency for the radial-inlet impeller installation of reference 5 as plotted against relative approach area and angle of attack is shown over a range of impeller-tip Mach numbers in figure 17. Peak efficiency for all impeller-tip Mach numbers occurred at values of relative approach area from about zero to 10 percent greater than the geometric area of the channel at the blade inlet (including blade thickness) corresponding to positive angles of attack from 3 to 6 degrees. Angle of attack is defined as the difference between the angle of the inlet air and the tangent to the blade mean line at the leading edge. The direction of the approaching fluid was calculated on the basis of inlet-depression tank stagnation conditions and the full area of the flow passage immediately upstream of the leading edge of the impeller blades. A 3-percent velocity-increase correction for shroud boundary-layer blockage and total-pressure loss was included.

16 NACA TN 2691

The over-all efficiency variation shown in figure 17 is a result of the combined effects of the various losses occurring in the flow. general, heavy contributors to impeller losses can be identified as (1) friction losses arising from the action of the mean flow on the wetted surface of the impeller and vaneless diffuser passages, (2) losses due to the somewhat sudden enlargement or contraction of the relative flow area across the blade inlet (referred to as inlet losses), (3) boundary-layer and secondary-flow losses due to the effects of blade-surface velocity gradients arising from the blade loading (referred to as blade-loading losses), and (4) shock losses due to supersonic velocities in the choked-flow range of operation. Friction losses depend principally on the square of the mean flow velocity and will, therefore, increase rapidly with increasing weight flow. Bladeloading losses, on the other hand, increase with decreasing weight flow as there is less kinetic energy available in the mean flow to overcome the adverse pressure gradients and boundary-layer growth imposed by the blade circulation. (For a radial discharge impeller with little slip, the circulation is approximately constant at a fixed tip speed.)

The relative magnitude of the inlet losses depends largely on whether the relative inlet area is contracting or expanding across the blade inlet. For low weight flows the flow area is enlarged (fig. 1), and from fluid mechanics for pipe flow (reference 9 or 10), the loss for sudden enlargement is given by (neglecting density changes)

$$F = \frac{V_1^2}{2g} \left( 1 - \frac{A_1}{A_2} \right)^2$$
 (19)

In this loss analysis, subscript 1 refers to conditions ahead of the blade leading edge and subscript 2 refers to conditions in the channel immediately downstream of the leading edge. For contracting areas at high weight flows,

$$F = \frac{KV_2^2}{2g}$$

where the factor K is a function primarily of area ratio. For values of  $A_2/A_1$  to about 0.5, the loss can be given approximately by

$$F = \frac{V_2^2}{2g} \left( 1 - \frac{A_2}{A_1} \right)^2$$
 (20)

Thus, as flow is decreased from the point of equal inlet area (minimum entrance loss), although the area ratio  $A_1/A_2$  decreases in equation (19), the relative inlet velocity  $V_1$  also decreases and the

NACA TN 2691 17

entrance losses will remain very small. In contrast, however, as flow is increased past the equal-area point,  $A_2/A_1$  decreases and  $V_2$  increases ( $V_2$  approaches the critical value) and a sharp rise in inlet loss occurs.

At a given impeller-tip speed, the composite loss picture in figure 17 is as follows: On the low weight-flow side of the equal-area point, friction losses decrease gradually, entrance losses remain very small, blade loading losses tend to increase and a gradual decline in efficiency to the surge point occurs. On the high weight-flow side, blade loading losses gradually decrease, but friction and inlet losses rise sharply to produce a rapid rate of decrease in efficiency to the choked flow point. The large declines in efficiency at the choked flows at the higher tip speeds are due to the shock losses of the supercritical passage flow.

The general decrease in efficiency as impeller-tip Mach number is increased (fig. 17) is a reflection of the increased friction and blade-loading losses resulting from the higher values of circulation and mean velocity at these wheel speeds. The decrease in range of operation at the higher tip speeds can also be attributed to the higher velocities and loadings. In the high flow region of operation, as the relative inlet Mach number is increased because of the higher wheel speeds, the area reduction necessary to cause a critical contraction ratio becomes progressively smaller.

At the choked flow point (local sonic velocity in the blade inlet region) the over-all efficiency is substantially greater at the higher wheel speeds than it is at the lower wheel speeds. The reduced overall efficiency at critical flow at low wheel speeds cannot be attributed to increased diffuser, friction, or blade-loading losses, because (1) impeller channel velocities are not substantially different for the various wheel speeds at the critical condition; (2) impeller blade loadings remain light at the lower wheel speeds; and (3) vaneless diffuser efficiency gives evidence of little change with wheel speed (references 11 and 12). A principal difference between the high- and lowspeed choking points however, is the flow-area change across the blade inlet. According to equation (20), with the velocities downstream of the area contraction approximately the same (local critical velocity), a greater inlet loss occurs at the lower wheel speeds where the inlet area change is the greatest. A similar condition of large inlet losses in the high flow range of a geometrically similar impeller at low wheel speeds was found in references 3 and 4.

In view of the indicated large inlet losses at negative angles of attack, improved performance and range of operation may be obtained if blade leading-edge shapes are designed for a more efficient accomodation of the inlet-flow variation.

#### SUMMARY OF RESULTS

From a theoretical analysis of the ideal one-dimensional flow in an illustrative rotating radial impeller channel with a convergent-divergent area, it was found that:

- 1. The behavior of the flow (variations of pressure, velocity, Mach number, etc.) along the radius of the rotating channel was generally similar in trend to that in a geometrically similar stationary nozzle.
- 2. Critical (sonic) conditions occurred upstream of the geometric throat, with the displacement from the throat increasing with increasing impeller wheel speed and with decreasing rate of area contraction.
- 3. The effect of losses on the variation of flow along the channel was similar to the effect of a reduction of the flow area.

A further one-dimensional analysis of the flow in an experimental radial-inlet impeller containing static-pressure taps along the stationary front shroud indicated that:

- 1. The behavior of the mean flow along the impeller passage was generally similar to that of flow along a rotating radial channel whose effective flow area at the inlet varies with the operating point.
- 2. A critical condition occurred in the inlet region of the impeller at high negative angles of attack where a throat is formed because of flow separation and readjustment downstream of the leading edge.
- 3. Calculated maximum weight flows based on conditions at the critical radius compared favorably with experimental maximum weight flows over the wheel speed range of the impeller.
- 4. Impeller-inlet losses were indicated to be large at the higher weight flows.

Lewis Flight Propulsion Laboratory
National Advisory Committee for Aeronautics
Cleveland, Ohio

## APPENDIX A

# LOGARITHMIC DIFFERENTIAL EQUATIONS

The variations of pressure, relative velocity, and relative Mach number along the radius of a channel can be obtained from equations (1) to (4) in the logarithmic differential form as follows.

Velocity. - From equation (4),

$$dt = \frac{1}{R} d\left(\frac{p}{\rho}\right) \tag{Al}$$

Substituting in equation (1) yields

$$VdV + \frac{c_p}{R} d\left(\frac{p}{\rho}\right) = dQ + d\left(\frac{\omega^2 r^2}{2}\right)$$

Differentiating  $p/\rho$ , with  $R = c_p - c_v$ , gives

$$VdV + \frac{\gamma}{\gamma - 1} \left[ \frac{dp}{\rho} - \left( \frac{p}{\rho} \right) \frac{d\rho}{\rho} \right] = dQ + d\left( \frac{\omega^2 r^2}{2} \right)$$
 (A2)

From continuity, equation (2),

$$\frac{\mathrm{d}\rho}{\rho} = -\frac{\mathrm{d}A}{A} - \frac{\mathrm{d}V}{V} \tag{A3}$$

Substituting for  $\frac{d\rho}{\rho}$  and  $\frac{dp}{\rho}$  in equation (A2) from equations (A3) and (3) yields, with  $a^2 = \gamma(\frac{p}{\rho})$ ,

$$-\frac{1}{\gamma-1}\frac{V^2dV}{V} + \frac{a^2}{\gamma-1}\frac{dV}{V} = dQ - \frac{1}{\gamma-1}d\left(\frac{\omega^2r^2}{2}\right) + \frac{\gamma}{\gamma-1}dF - \frac{a^2}{\gamma-1}\frac{dA}{A}$$

Multiplying through by  $\frac{\gamma-1}{a^2}$ , using  $M^2 = \frac{V^2}{a^2}$  and condensing give

$$\frac{dV}{V} = -\frac{1}{1-M^2} \left\{ \frac{1}{a^2} \left[ d \left( \frac{\omega^2 r^2}{2} \right) - \gamma dF - (\gamma - 1) dQ \right] + \frac{dA}{A} \right\}$$
 (6)

<u>Pressure.</u> - From equation (3), using  $a^2 = \frac{\gamma p}{\rho}$  and equation (6) yields

$$\frac{\mathrm{dp}}{\mathrm{p}} = \frac{\gamma}{1-\mathrm{M}^2} \left( \frac{1}{\mathrm{a}^2} \left[ \mathrm{d} \left( \frac{\omega^2 \mathrm{r}^2}{2} \right) - \left[ (\gamma - 1) \mathrm{M}^2 + 1 \right] \right] + \left[ (\gamma - 1) \mathrm{M}^2 \right] + \left$$

Mach number. - From the definition of Mach number M = V/a it can be shown that

$$\frac{\mathrm{dM}}{\mathrm{M}} = \frac{\mathrm{dV}}{\mathrm{V}} - \frac{1}{2} \cdot \frac{\mathrm{da}^2}{\mathrm{a}^2} \tag{A4}$$

From the definition of sonic velocity,

$$da^2 = \gamma d\left(\frac{p}{\rho}\right) = a^2 \left(\frac{dp}{p} - \frac{d\rho}{\rho}\right)$$
 (A5)

Thus, equation (A4) can be expressed as

$$\frac{\mathrm{d}M}{M} = \frac{\mathrm{d}V}{V} - \frac{1}{2} \left( \frac{\mathrm{d}p}{p} - \frac{\mathrm{d}\rho}{\rho} \right) \tag{A6}$$

Substituting for  $\frac{d\rho}{\rho}$  from equation (A3) gives

$$\frac{dM}{M} = \frac{1}{2} \left( \frac{dV}{V} - \frac{dp}{p} - \frac{dA}{A} \right) \tag{A7}$$

Substituting for  $\frac{dV}{V}$  and  $\frac{dp}{p}$  in equation (A7) from equation (6) and (5) then yields after combining terms

(7)

$$\frac{dM}{M} = -\frac{1}{2(1-M^2)} \left( \frac{1}{a^2} \left\{ (1+\gamma) d \left( \frac{\omega^2 r^2}{2} \right) - \frac{1}{2(1-M^2)} dF - (\gamma-1)(1+\gamma M^2) dQ \right\} + \left[ 2 + (\gamma-1) M^2 \right] \frac{dA}{A} \right)$$

#### APPENDIX B

#### IDEAL MAXIMUM MASS FLOW

From continuity, the ideal mass flow at any cross section of a channel for one-dimensional flow is given by

$$W = \rho VA \tag{Bl}$$

From the energy equation

$$V = \left[2c_p JT_0 + \omega^2 r^2 - \left(\frac{2\gamma}{\gamma - 1}\right) \frac{p}{\rho}\right]^{\frac{1}{2}}$$
(B2)

From the isentropic relation for ideal flow

$$\rho = \rho_{O} \left( \frac{p}{P_{O}} \right)^{\Upsilon}$$
 (B3)

Thus,

$$\frac{\gamma}{\gamma - 1} \frac{p}{\rho} = \frac{\gamma}{\gamma - 1} \frac{P_O}{\rho_O} \left(\frac{p}{P_O}\right)^{\frac{\gamma - 1}{\gamma}}$$
(B4)

Now, inasmuch as

$$\gamma \frac{P_0}{\rho_0} = a_0^2$$

equation (B4) can be expressed as

$$\frac{\gamma}{\gamma - 1} \frac{p}{\rho} = \frac{a_o^2}{\gamma - 1} \left(\frac{p}{P_o}\right)^{\frac{\gamma - 1}{\gamma}}$$
(B5)

Furthermore, from the perfect gas law,

$$c_p JT_o = \frac{\gamma}{\gamma - 1} \frac{P_o}{\rho_o} = \frac{a_o^2}{\gamma - 1}$$
 (B6)

Substituting equations (B2), (B3), (B5), and (B6) into equation (B1) results in

$$W = \rho_{o} \left(\frac{p}{P_{o}}\right)^{\frac{1}{\gamma}} A \left[\frac{2}{\gamma-1} a_{o}^{2} + \omega^{2} r_{T}^{2} \left(\frac{r}{r_{T}}\right)^{2} - \frac{2a_{o}^{2}}{\gamma-1} \left(\frac{p}{P_{o}}\right)^{\frac{\gamma-1}{\gamma}}\right]^{\frac{1}{2}}$$

from which is obtained

$$W = \sqrt{\frac{2}{\gamma - 1}} a_{O} \rho_{O} A \left\{ \left[ 1 + \frac{\gamma - 1}{2} \left( \frac{\mathbf{r}}{r_{T}} \right)^{2} M_{T} \right] \left( \frac{\mathbf{p}}{P_{O}} \right)^{\frac{2}{\gamma}} - \left( \frac{\mathbf{p}}{P_{O}} \right)^{\frac{\gamma + 1}{\gamma}} \right\}^{\frac{1}{2}}$$
(B7)

Differentiating W with respect to pressure ratio at a given crosssectional area yields

$$\frac{\partial W}{\partial \left(\frac{p}{P_o}\right)} = \sqrt{\frac{2}{\gamma - 1}} \, a_o \rho_o \, A \, \frac{\frac{1}{2} \left\{\frac{2}{\gamma} \left[1 + \frac{\gamma - 1}{2} \left(\frac{r}{r_T}\right)^2 M_T^2\right] \left(\frac{p}{P_o}\right)^{\frac{2 - \gamma}{\gamma}} - \frac{\gamma + 1}{\gamma} \left(\frac{p}{P_o}\right)^{\frac{1}{\gamma}}\right\}}{\left\{\left[1 + \frac{\gamma - 1}{2} \left(\frac{r}{r_T}\right)^2 M_T^2\right] \left(\frac{p}{P_o}\right)^{\frac{2}{\gamma}} - \left(\frac{p}{P_o}\right)^{\frac{\gamma + 1}{2}}\right\}^{\frac{1}{2}}}$$

Inasmuch as the denominator is a nonzero quantity (see equation (B7)), it is sufficient to set only the term between braces in the numerator equation zero in order to maximize equation (B7), or

$$\frac{2}{\gamma} \left[ 1 + \frac{\gamma - 1}{2} \left( \frac{\mathbf{r}}{\mathbf{r}_{\mathrm{T}}} \right)_{\mathrm{m}}^{2} M_{\mathrm{T}}^{2} \right] \left( \frac{\mathbf{p}}{\mathbf{p}_{\mathrm{o}}} \right)_{\mathrm{m}}^{2} - \frac{\gamma + 1}{\gamma} \left( \frac{\mathbf{p}}{\mathbf{p}_{\mathrm{o}}} \right)_{\mathrm{m}}^{2} = 0$$
 (B8)

from which the pressure ratio at maximum flow is obtained as

$$\left(\frac{\underline{p}}{\underline{p}_{o}}\right)_{m} = \left[\frac{2}{\gamma+1} + \frac{\gamma-1}{\gamma+1} \left(\frac{\underline{r}}{\underline{r}_{T}}\right)_{m}^{2} M_{T}^{2}\right]^{\frac{\gamma}{\gamma-1}}$$
(B12)

The velocity at the maximum flow condition is found by expressing equation (B2) in terms of the local velocity of sound

$$V_{\rm m} = \sqrt{\frac{2}{\gamma - 1}} a_{\rm o} \left[ 1 + \frac{\gamma - 1}{2} \left( \frac{r}{r_{\rm T}} \right)_{\rm m}^2 M_{\rm T}^2 - \frac{a_{\rm m}^2}{a_{\rm o}^2} \right]^{\frac{1}{2}}$$

Then, from equation (B8)

$$V_{m} = \sqrt{\frac{2}{\gamma - 1}} a_{o} \begin{bmatrix} \frac{\gamma - 1}{2} & \frac{2}{2} \\ \frac{p}{P_{o}} \end{pmatrix}_{m}^{\gamma} & \frac{a_{m}^{2}}{a_{o}^{2}} \end{bmatrix}^{\frac{1}{2}}$$
(B9)

Substituting the adiabatic relation

$$\left(\frac{p}{P_{o}}\right)_{m}^{\frac{\gamma-1}{2\gamma}} = \frac{a_{m}}{a_{o}}$$

into equation (B9) and rearranging give

$$V_{m} = \left(\frac{\gamma + 1}{\gamma - 1} a_{m}^{2} - \frac{2}{\gamma - 1} a_{m}^{2}\right)^{\frac{1}{2}}$$

from which is obtained the critical condition

$$V_{m} = a_{c}$$

Thus the maximum mass flow occurs at the critical condition and all m subscripts can be replaced by c subscripts.

The maximum mass flow is given by

$$W = \rho_C a_C A_C$$

which becomes, after the introduction of the isentropic and sonic relations

$$W_{\rm m} = \rho_{\rm O} \, a_{\rm O} \, A_{\rm C} \left(\frac{p}{P_{\rm O}}\right)_{\rm C}$$
 (B10)

Substituting for the critical pressure ratio from equation (12)

$$\frac{W_{\rm m}}{\rho_{\rm o}a_{\rm o}A_{\rm c}} = \psi_{\rm m} = \left\{ \frac{2}{\gamma+1} \left[ 1 + \frac{\gamma-1}{2} \left( \frac{r}{r_{\rm T}} \right)_{\rm c}^2 M_{\rm T}^2 \right] \right\}^{\frac{\gamma+1}{2(\gamma-1)}} \tag{13}$$

## APPENDIX C

# MASS-FLOW CHOKING LINE FOR FLOW WITH LOSSES

Maximum mass flow in a rotating channel in the presence of losses can be obtained as follows.

From continuity, at the critical condition

$$W_{c}' = \rho_{c}' a_{c}' A_{c}' \tag{C1}$$

With the use of the sonic relation and equation of state,

$$W_{c}^{\dagger} = \frac{p_{c}^{\dagger} \sqrt{\gamma R}}{R \sqrt{t_{c}^{\dagger}}} A_{c}^{\dagger}$$
 (C2)

From the energy equation for relative flow,

$$c_p J t_c + \frac{a_c^2}{2} = c_p J T_o + \frac{\omega^2 r_c^2}{2}$$

or

$$c_p J t_c + \frac{\gamma R t_c}{2} = c_p J T_o + \frac{\omega^2 r_c^2}{2}$$

from which

$$t_{c} = \frac{2}{\gamma + 1} T_{o} \left( 1 + \frac{\gamma - 1}{2} \frac{\omega^{2} r_{c}^{2}}{a_{o}^{2}} \right)$$

or

$$t_{c} = \frac{2}{\gamma + 1} T_{o} \left[ 1 + \frac{\gamma - 1}{2} \left( \frac{r_{c}}{r_{T}} \right)^{2} M_{T}^{2} \right]$$
 (C3)

Substituting equation (C3) into equation (C2) gives

$$W_{c}^{!} = \frac{\frac{P_{c}^{!}}{P_{o}} \sqrt{\gamma RT_{o}} A_{c} P_{o}}{RT_{o} \sqrt{\frac{2}{\gamma+1} \left[1 + \frac{\gamma-1}{2} \left(\frac{r_{c}^{!}}{r_{T}}\right)^{2} M_{T}^{2}\right]}}$$

and

$$\frac{\mathbf{W_c^{'}}}{\mathbf{a_0} \, \rho_0 \, \mathbf{A_c}} = \mathbf{\psi_c^{'}} = \frac{\left(\frac{\mathbf{p'}}{\mathbf{P_0}}\right)_{\mathbf{c}}}{\sqrt{\frac{2}{\gamma + 1} \left[1 + \frac{\gamma - 1}{2} \left(\frac{\mathbf{r_c^{'}}}{\mathbf{r_T}}\right)^2 \, \mathbf{M_T}^2\right]}}$$
(C4)

The isentropic critical mass-flow function is obtained from equation (BlO) as

$$\psi_{c} = \left(\frac{p}{P_{o}}\right)_{c} \left(\frac{p}{P_{o}}\right)_{c}$$
(C5)

and from equation (12) for critical pressure ratio

$$\psi_{c} = \frac{\left(\frac{p}{P_{o}}\right)_{c}}{\sqrt{\frac{2}{\gamma+1}\left[1 + \frac{\gamma-1}{2}\left(\frac{r}{r_{T}}\right)_{c}^{2} M_{T}^{2}\right]}}$$
(C6)

The ratio of actual to isentropic critical mass-flow function or choking line thus becomes

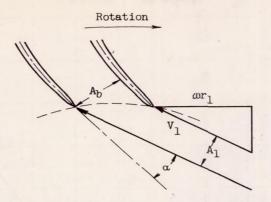
$$\frac{\psi_{c}^{\prime}}{\psi_{c}} = \frac{\left(\frac{p^{\prime}}{P_{o}}\right)_{c} \sqrt{1 + \frac{\Upsilon-1}{2} \left(\frac{\mathbf{r}}{r_{T}}\right)_{c}^{2} M_{T}^{2}}}{\left(\frac{p}{P_{o}}\right)_{c} \sqrt{1 + \frac{\Upsilon-1}{2} \left(\frac{\mathbf{r}^{\prime}}{r_{T}}\right)_{c}^{2} M_{T}^{2}}}$$
(15)

#### REFERENCES

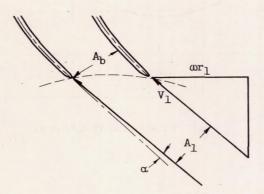
- 1. Ellis, Gaylord O., and Stanitz, John D.: Two-Dimensional Compressible Flow in Centrifugal Compressors with Logarithmic-Spiral Blades. NACA TN 2255, 1951.
- 2. Stanitz, John D., and Ellis, Gaylord O.: Two-Dimensional Compressible Flow in Centrifugal Compressors with Straight Blades. NACA Rep. 954, 1950. (Formerly NACA TN 1932.)

- 3. Michel, Donald J., Ginsburg, Ambrose, and Mizisin, John: Experimental Investigation of Flow in the Rotating Passages of a 48-Inch Impeller at Low Tip Speeds. NACA RM E51D20, 1951.
- 4. Prian, Vasily D., and Michel, Donald J.: An Analysis of the Flow in Rotating Passage of Large Radial-Inlet Centrifugal Compressor at Tip Speed of 700 Feet per Second. NACA TN 2584, 1951.
- 5. Johnsen, I. A., Ritter, W. K., and Anderson, R. J.: Performance of a Radial-Inlet Impeller Designed on the Basis of Two-Dimensional-Flow Theory for an Infinite Number of Blades. NACA TN 1214, 1947.
- 6. Stanitz, J. D., and Prian, Vasily D.: A Rapid, Approximate Method for Determining Velocity Distribution on Impeller Blades of Centrifugal Compressors. NACA TN 2421, 1951.
- 7. Hicks, Bruce L., Montgomery, Donald J., and Wasserman, Robert H.:
  The One-Dimensional Theory of Steady Compressible Fluid Flow in
  Ducts with Friction and Heat Addition. NACA TN 1336, 1947.

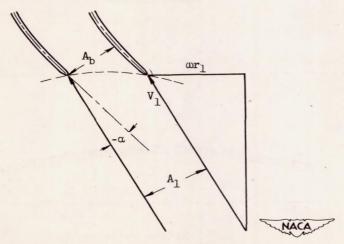
  (Formerly NACA ARR E6E22.)
- 8. Emmons, Howard W.: Shock Waves in Aerodynamics. Jour. Aero. Sci., vol. 12, no. 2, April 1945, pp. 188-194.
- 9. Vennard, John K.: Elementary Fluid Mechanics. John Wiley & Sons, Inc., 2d ed., 1947, pp. 174-177.
- 10. Dodge, Russell A., and Thompson, Milton J.: Fluid Mechanics. McGraw-Hill Book Co., Inc., 1937, pp. 212-215.
- ll. Barina, Frank J.: Comparative Performance of Two Vaneless Diffusers
  Designed with Different Rates of Passage Curvature for Mixed-Flow
  Impellers. NACA TN 1490, 1947.
- 12. Bradshaw, Guy R., and Laskin, Eugene B.: Experimental Study of Effect of Vaneless-Diffuser Diameter on Diffuser Performance. NACA TN 1713, 1948.



(a) Approach area less than blade area (low weight flow).

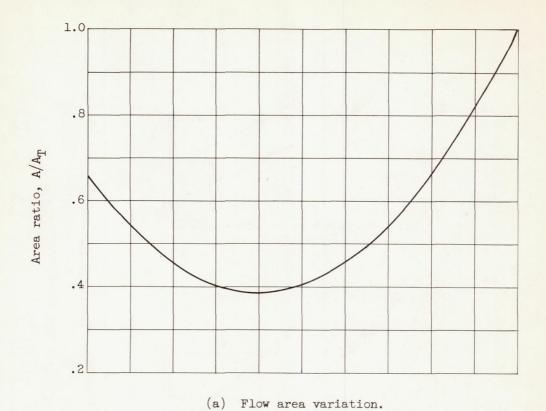


(b) Approach area equal to blade area (medium weight flow).

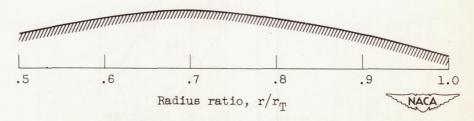


(c) Approach area greater than blade area (high weight flow).

Figure 1. - Variation of relative approach area over weight-flow range of impeller operation.







(b) Equivalent circular nozzle.

Figure 2. - Illustrative impeller channel for theoretical flow analysis.

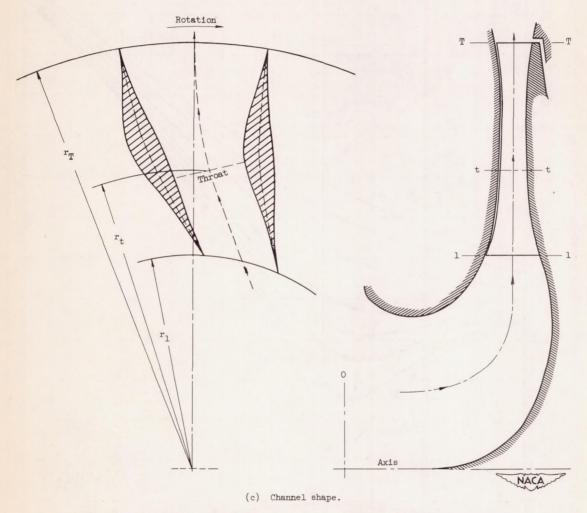


Figure 2. - Concluded. Illustrative impeller channel for theoretical flow analysis.

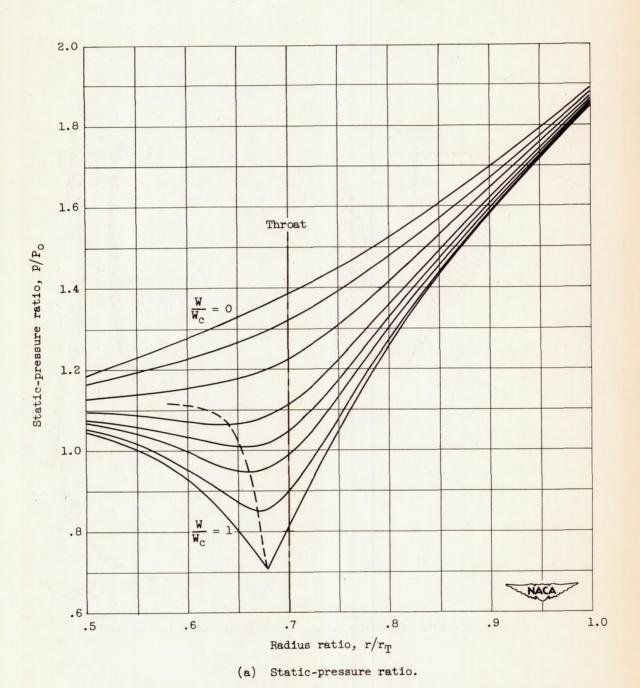


Figure 3. - Variation of flow along illustrative impeller channel from zero to critical flow. Impeller-tip Mach number  $M_{\rm T}$ , 1.0.

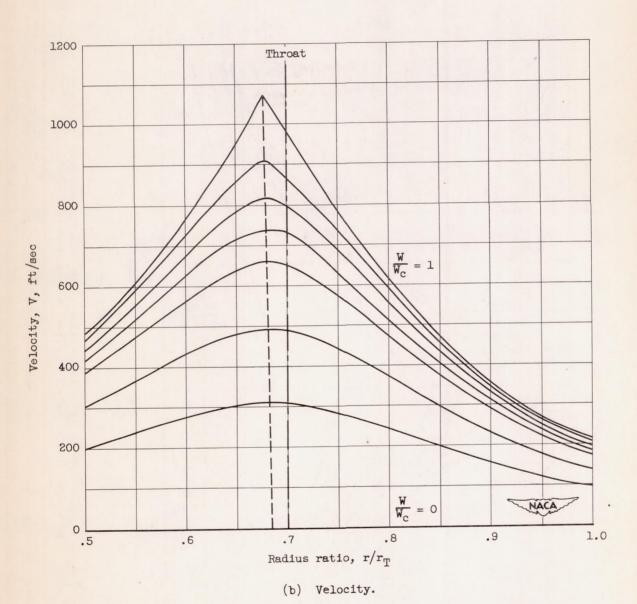
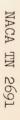


Figure 3. - Continued. Variation of flow along illustrative impeller channel from zero to critical flow. Impeller-tip Mach number  $M_{\rm T}$ , 1.0.



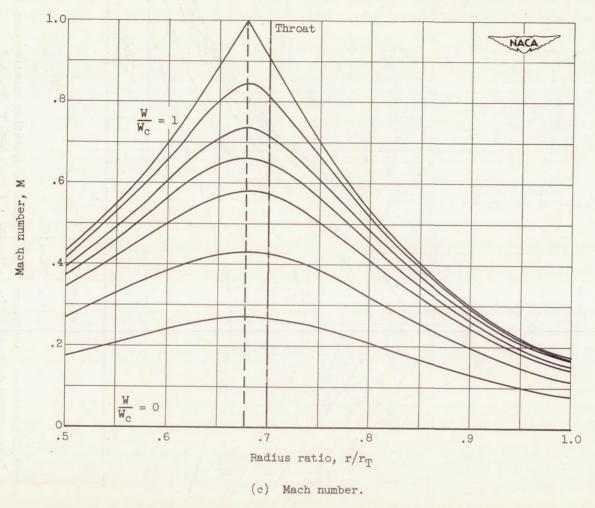


Figure 3. - Concluded. Variation of flow along illustrative impeller channel from zero to critical flow. Impeller-tip Mach number  $\,\mathrm{M}_{\mathrm{T}},$  1.0.

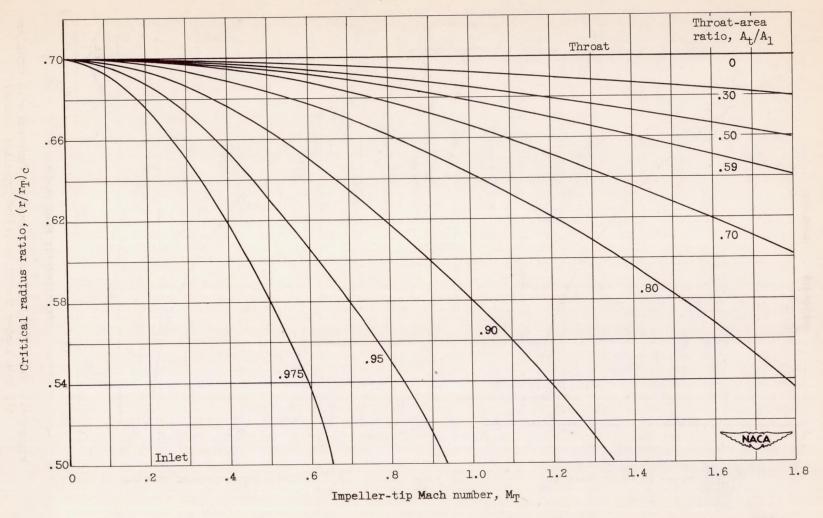


Figure 4. - Variation of critical radius ratio with impeller-tip Mach number for various throat-area ratios (constant throat area).

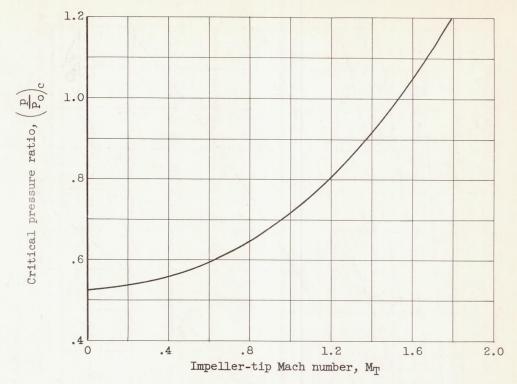


Figure 5. - Variation of critical pressure ratio with impellertip Mach number for illustrative impeller channel.

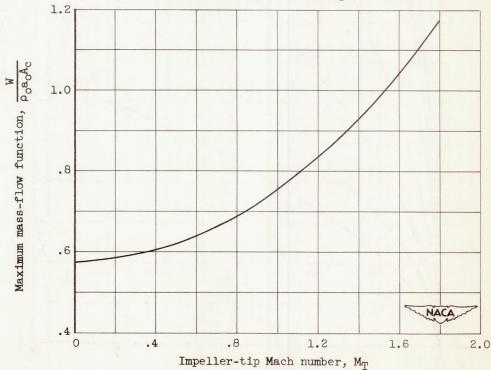


Figure 6. - Variation of maximum mass-flow function with impellertip Mach number for illustrative impeller channel.

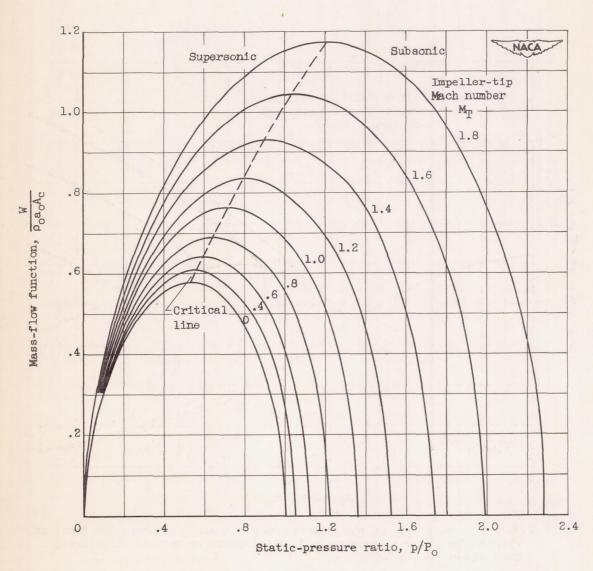


Figure 7. - Variation of mass-flow function with pressure ratio at critical radius for illustrative impeller channel.

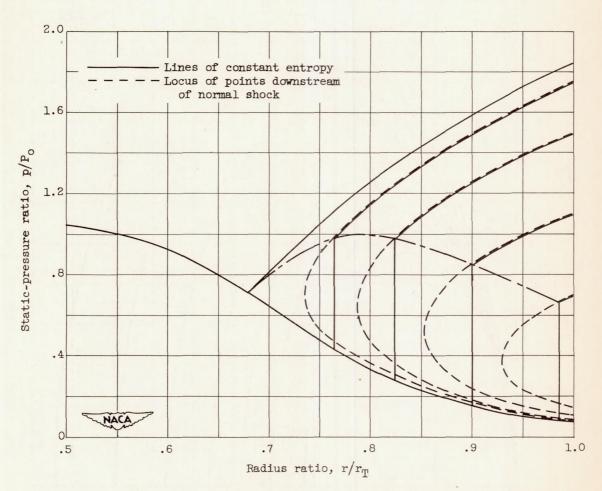


Figure 8. - Variation of static-pressure ratio along illustrative impeller channel for several supercritical outlet-pressure ratios. Impeller-tip Mach number  $M_{\rm T}$ , 1.0.

NACA TN 2691

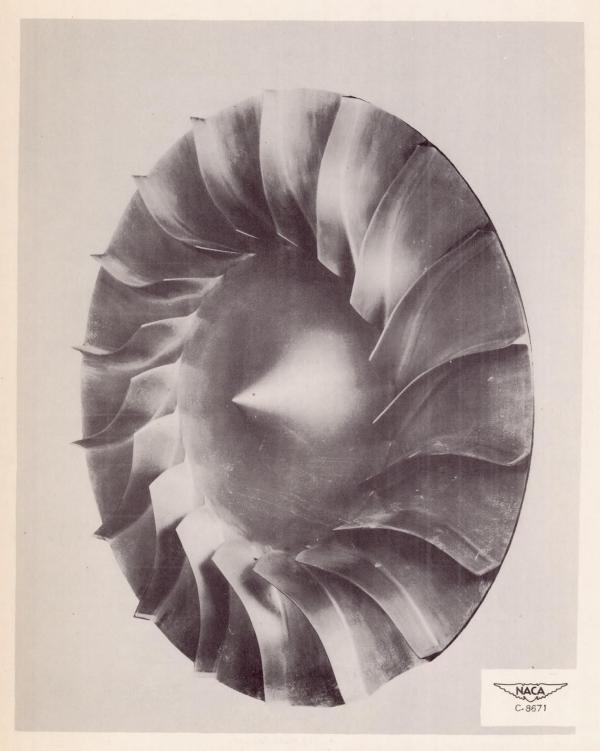


Figure 9. - Experimental radial-inlet impeller (reference 5).

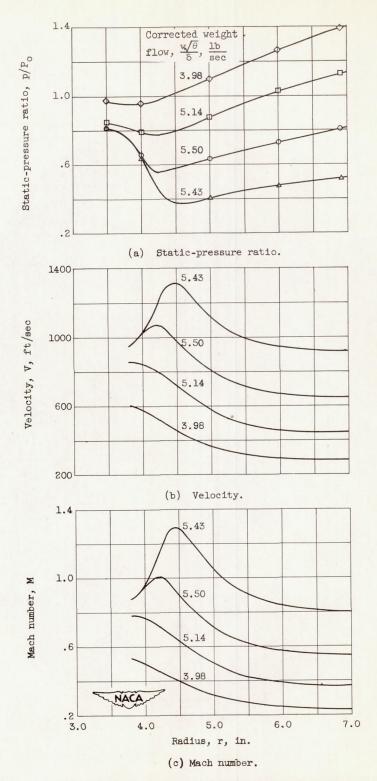


Figure 10. - Measured variations of shroud static pressure and calculated variations of velocity and Mach number along channel of experimental radial-inlet impeller. Impeller-tip Mach number, 0.878.

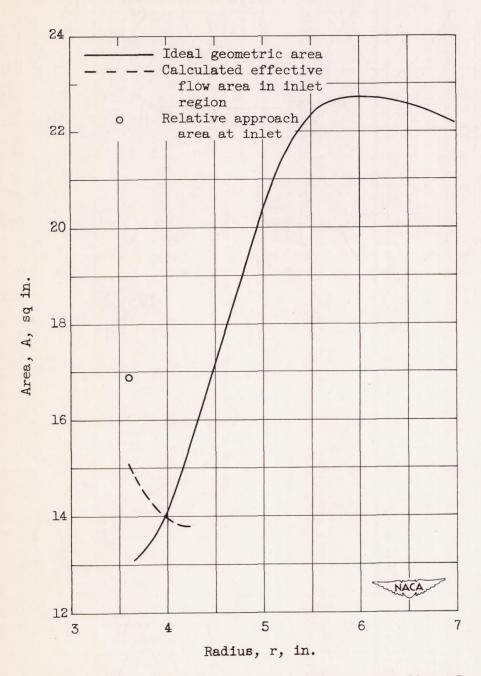


Figure 11. - Variation of flow area along radius of experimental radial-inlet impeller at maximum weight flow. Impeller-tip Mach number M<sub>T</sub>, 0.878.

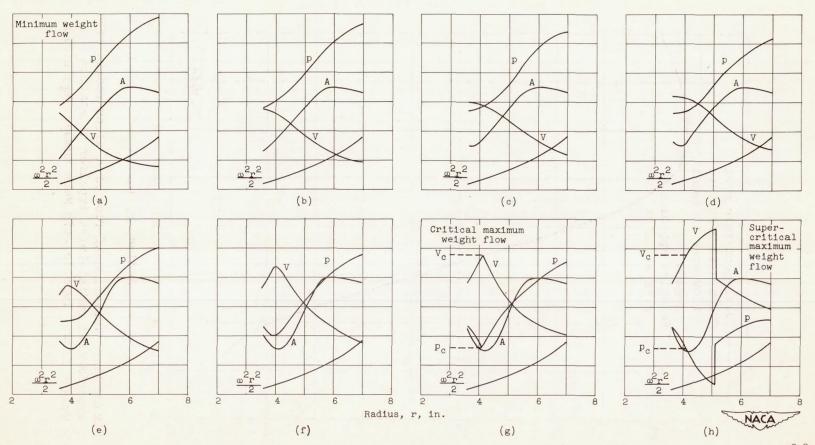


Figure 12. - Qualitative variation of one-dimensional effective flow area A, static pressure p, velocity V, and potential energy along channel of experimental radial-inlet impeller as flow is increased from minimum to maximum at constant impeller-tip speed.

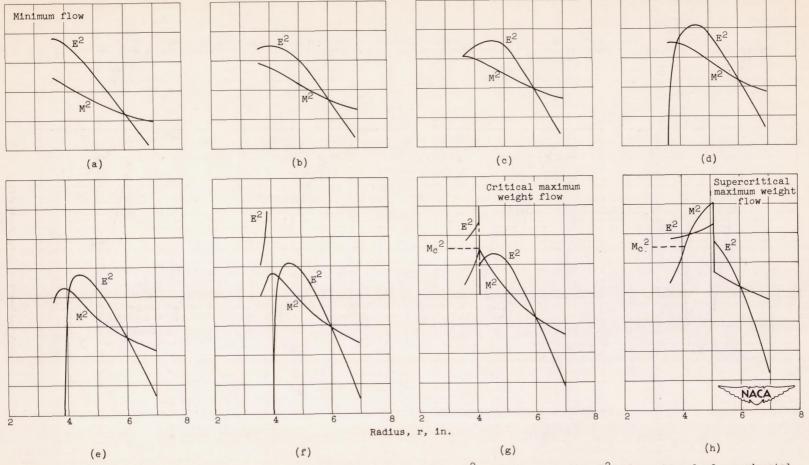


Figure 13. - Qualitative one-dimensional variation of square of Mach number  $M^2$  and energy number  $E^2$  along channel of experimental radial-inlet impeller as flow is increased from minimum to maximum at constant impeller-tip speed.

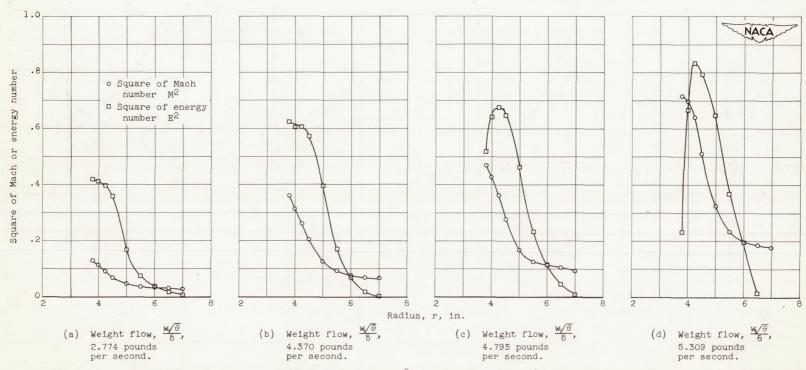


Figure 14. - Calculated variations of square of Mach number  $M^2$  and energy number  $E^2$  along channel of experimental radial-inlet impeller as flow is increased from minimum to maximum. Impeller-tip Mach number  $M_T$ , 0.878.

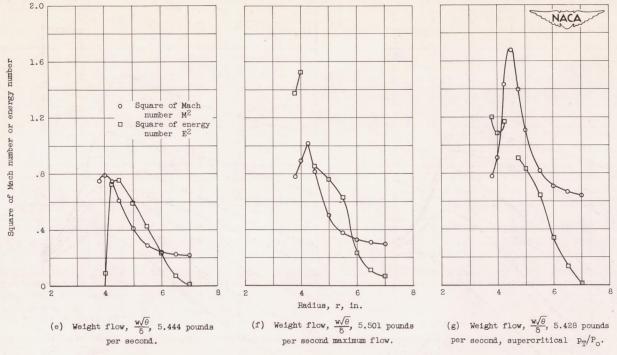


Figure 14. - Concluded. Calculated variations of square of Mach number  $M^2$  and energy number  $E^2$  along channel of experimental radial-inlet impeller as flow is increased from minimum to maximum. Impeller-tip Mach number  $M_{\rm T}$ , 0.878.

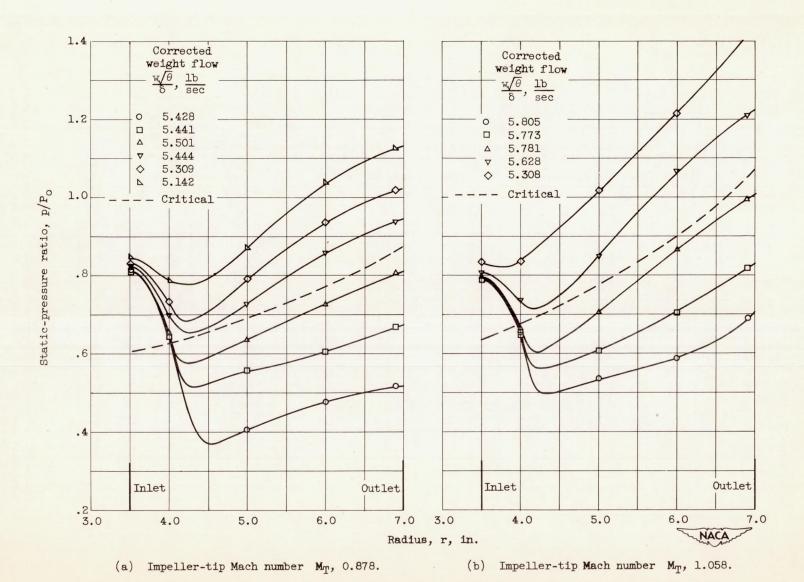


Figure 15. - Variation of static-pressure ratio along radius of experimental radial-inlet impeller.

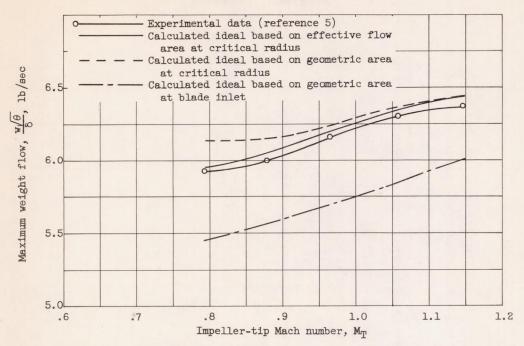


Figure 16. - Variation of maximum weight flow with impeller-tip Mach number for experimental radial-inlet impeller.

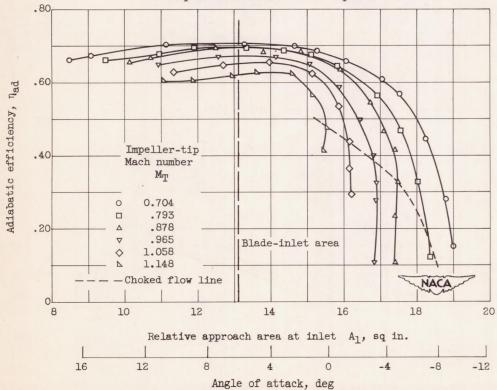


Figure 17. - Variation of over-all adiabatic efficiency with relative approach area and angle of attack at inlet of experimental radial-inlet impeller.